

# First-principles calculations of the vibrational properties of bulk CdSe and CdSe nanowires

M. Mohr<sup>1,\*</sup> and C. Thomsen<sup>1</sup>

<sup>1</sup>*Institut für Festkörperphysik, Technische Universität Berlin, Hardenbergstr. 36, 10623 Berlin, Germany*

(Dated: February 6, 2020)

We present first-principles calculations on the structural, electronic and vibrational properties of small diameter CdSe nanowires depending on size and surface termination. The evolution of phonon frequencies with decreasing diameter is analyzed. We find strongly size-dependent and nearly constant modes. We predict a low-frequency, diameter-dependent radial breathing mode (RBM) in CdSe nanowires.

PACS numbers: 31.15.E-,61.72.uj, 63.22.-m, 63.22.Gh

## I. INTRODUCTION

Nanostructures have become an important field in solid state physics. Much information on the characteristics of these systems can be gained from their vibrational properties. CdSe as a direct semiconductor with strong size-tunable properties is widely used in nanostructures. Still little efforts have been made to analyze its lattice dynamics or the effect of confinement.<sup>1,2</sup> To our knowledge no calculation of the vibrational properties in the hexagonal plane of the Brillouin zone is available for CdSe. The importance of these properties was demonstrated for carbon nanotubes; Raman experiments, that directly measure phonon frequencies, are now a standard tool for the determination of tube diameter and chirality.<sup>3</sup> These achievements however required a solid theoretical basis, which first-principles calculations have shown to be.

In the present work we concentrate on the vibrational properties of CdSe bulk and nanowires (NWs). We compare six nanowires with diameters between 5 and 20 Å, divided into two categories, hexagon-shaped and triangle-shaped wires. Structural and electronic properties depending on the diameter and surface termination are investigated. We show how the counterparts of the optical bulk modes evolve in frequency with decreasing diameter. Finally, we predict a low-frequency radial breathing mode (RBM) that is strongly size-dependent.

## II. CALCULATIONAL DETAILS

Two different DFT codes were used for the calculation of bulk properties and nanowire properties: for the phonon dispersion of bulk material we used linear response, which is implemented in ABINIT.<sup>4,5,6,7</sup> For large unit cells, as required by one-dimensional systems, however, plane wave basis sets are computationally very expensive. Therefore we used the SIESTA code that uses a localized basis set for nanowires.<sup>8,9</sup>

The nanowires were generated by cutting appropriate discs out of a wurtzite crystal. The cross section of the relaxed unit cells is shown in Fig. 1. We used the LDA functional of Perdew and Zunger<sup>11</sup> in SIESTA and Troullier-Martins<sup>12</sup> pseudopotentials. The *4d* electrons of Cd were taken as valence electrons. The valence electrons were described by a double- $\zeta$  basis set plus an additional polarizing orbital. Periodic images of the NWs were separated by at least 20 Å. An

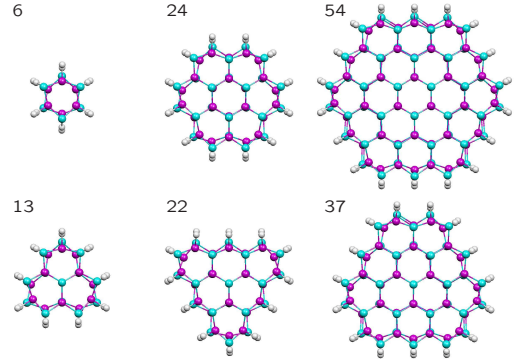


FIG. 1: (Color online) Left: Cross sections of all calculated hydrogen-coated nanowires. Number of CdSe-pairs is printed. As can be seen, near the surface, the Cd atoms (magenta, dark) move more inwards, as compared to bulk region.<sup>10</sup>

equivalent energy cutoff of 80 Ry was used for the real space grid integrations in all calculations. For bulk CdSe a  $(6 \times 6 \times 4)$  Monkhorst-Pack<sup>13</sup> mesh in reciprocal space was used, whereas for wires a minimum of 8  $k$ -points equally spaced within the Brillouin zone was used. The phonon calculations were performed with the method of finite-differences.<sup>14</sup> For the calculation of the LO splitting we used the experimental dielectric high-frequency constant<sup>15</sup>  $\epsilon_{\infty}^{\parallel} = 6.0$  and a modified version of SIESTA described in Ref.16.

The lattice parameters for wurtzite CdSe obtained with ABINIT were  $a=4.29$  Å and  $c=7.00$  Å; SIESTA yields  $a=4.34$  Å and  $c=7.09$  Å, both in good agreement with the experimental values  $a=4.2999$  Å and  $c=7.0109$  Å from inelastic neutron scattering (INS).<sup>2</sup> We also calculated the bulk modulus and obtained the values 55.58 GPa (ABINIT) and 55.54 GPa (SIESTA) again in good agreement with the experimental value 53.4 GPa.<sup>17</sup>

Symmetry considerations helped to reduce the calculation time. Nanowires can be described in terms of line groups,<sup>18</sup> which are the one-dimensional analogon to space groups. The NWs from Fig. 1 with a hexagon in the center (upper row) belong to the line group  $L(6)_3mc$  which has the generator  $\{C_6|t/2\}$ . This manifests itself in a screw axis. The NWs from Fig. 1 with three 120° bonds in the center (lower row) belong to the line group  $L3m$  which has the generator  $\{C_3|0\}$ . We did not only apply symmetry operation to the resulting

force constants but also beforehand in the relaxation process. This was done in the following way: After the NW was relaxed, we generated the whole wire by applying symmetry operations to a minimal set of atoms in the unit cell. This symmetry generated cell was relaxed again. This iterative process was repeated until all forces were below  $0.04 \text{ eV/\AA}$  after generating the wire. Although the relaxation process is considered to not change the symmetry we observed better results with the generating method: Frequencies of phonons belonging to two-dimensional representations (degenerate frequencies) were separated by less than  $0.05 \text{ cm}^{-1}$ .

### III. RESULTS AND DISCUSSION

The unit cell length  $c$  of the nanowires changes with diameter and with the addition of a hydrogen passivation shell around them. We plotted the unit cell length  $c$  over the inverse diameter  $1/d$  in Fig. 2. The diameter is defined by the distance of the outermost Cd or Se atom neglecting H atoms to the rotational. The bare wires have larger unit cell parameter  $c$  than the passivated NWs. The largest increase of 3.5 % was found for the  $(\text{CdSe})_{13}$  wire. For the largest wire discussed here, the  $(\text{CdSe})_{54}$ , the increase is 1.7 %. We find linear relationship, which is best described by the parameters  $c_{\text{NW}}(d) = c - m/d$  with the bulk lattice constant  $c = 7.09 \text{ \AA}$  and  $m = 3.26 \text{ \AA}^2$  (passivated) and  $m = 1.75 \text{ \AA}^2$  (bare) nanowires.

The surface of all calculated structures undergo a reconstruction, the H-passivation does not qualitatively change the reconstruction. This reconstruction was found experimentally for wires by extended x-ray absorption fine structure spectroscopy.<sup>10</sup> During this reconstruction the Cd-atoms rotate into the surface to lower the energy as can be seen in Fig. 1. After relaxation, the Cd-Se bonds show a broad distribution in lengths. In the core the bond lengths deviate from the bulk value by  $< 1\%$ , while those on the surface change by up to  $5\%$ . The change in bond length causes changes in the force constants which will be discussed later.

CdSe has a direct electronic band gap. It is known from absorption or photoluminescence measurements that the band gap of CdSe nanocrystallites and nanowires shows a strong size dependence.<sup>19</sup> In Fig. 2 (lower) we plot the band gap increase (compared to the calculated bulk value) over the inverse diameter. As can be seen the passivation influences the electronic band structure; it generally increases the band gap at the  $\Gamma$  point. At first sight this is a strange behavior as the H-atoms add electronic states to the unit cell. However, at the same time the lattice parameter  $c$  decreases with the addition of the H-atoms which is a stronger effect. Thus the lateral confinement increases and leads to a net increase of the band gap. The data from the wires with passivation is in excellent agreement with the shown semiempirical pseudopotential calculation (SPC) data from Ref. 19 that are based on experimental data.

The phonon dispersion calculated with ABINIT is shown in Fig. 3. Also shown are experimental frequencies obtained with INS along the  $\Gamma$ -A direction which was multiplied by  $\sqrt{(116/112.4)}$  to account for the use of  $^{116}\text{Cd}$  isotope instead

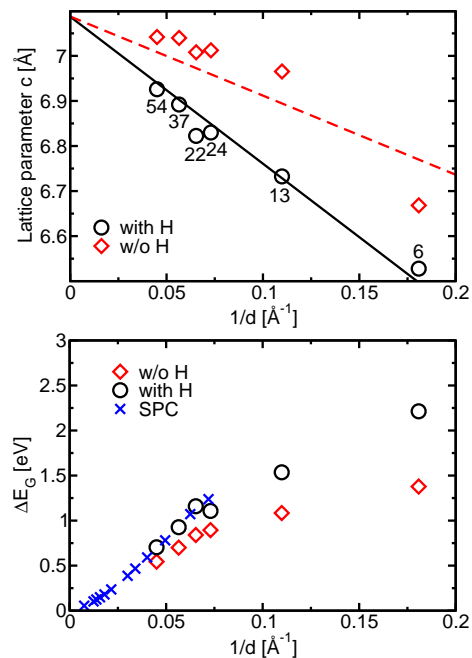


FIG. 2: (Color online) Upper: Evolution of the unit cell lengths of the nanowires with and without H-atoms. Bulk CdSe is considered as an inverse diameter of 0. The number of CdSe-pairs is indicated. Lower: Electronic transition energy difference (compared to bulk) at the  $\Gamma$ -point of the nanowires with and without H-passivation. Crosses denote data from semiempirical pseudopotential calculation (SPC) from Ref. 19.

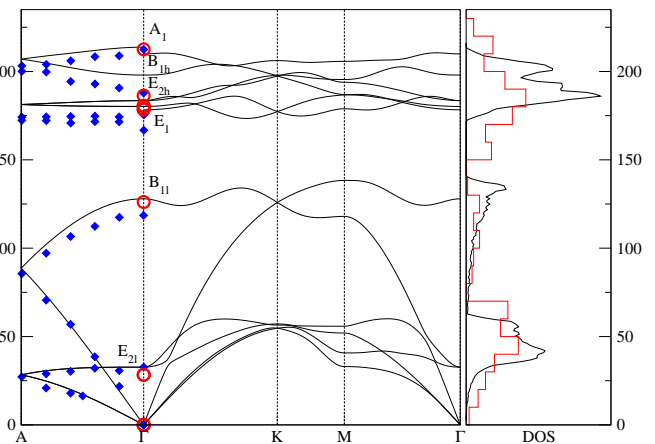


FIG. 3: (Color online) Phonon dispersion curves and DOS for bulk CdSe as calculated with ABINIT (solid lines). Diamonds are experimental data from Ref. 2. Circles are  $\Gamma$ -point frequencies calculated with SIESTA. In the bulk phonon DOS (line) we plotted the  $\Gamma$ -DOS of the ideal  $(\text{CdSe})_{54}$ -wire (histogram).

of natural Cd with an atomic weight of  $112.4 \text{ U}$ .<sup>2</sup> The  $\Gamma$ -point phonons calculated with SIESTA are also plotted; we compare them later with the nanowire frequencies. All frequencies were multiplied by a constant factor to match the experimental bulk LO frequency at the  $\Gamma$ -point. The dispersion along  $\Gamma - K$  and  $\Gamma - M$  shows an overbending near the  $\Gamma$ -point, which can

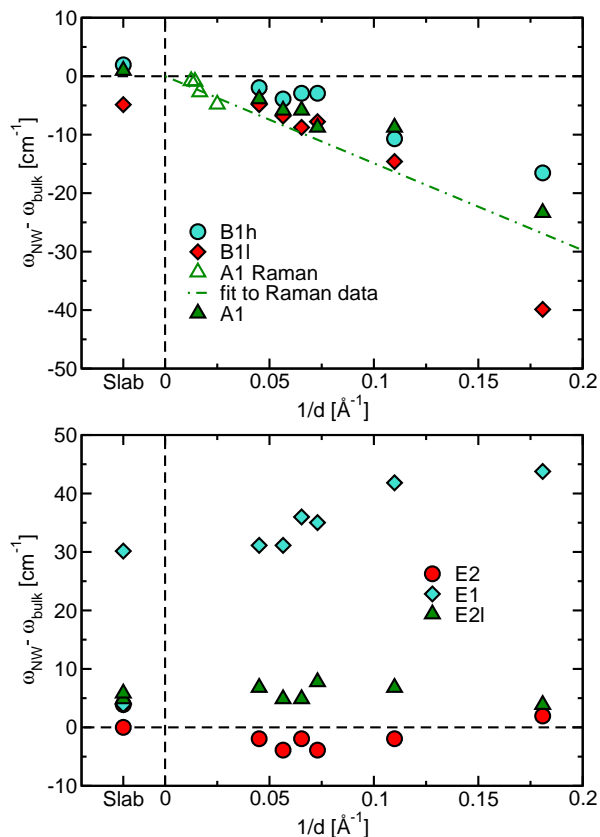


FIG. 4: (Color online) Phonon energy difference  $\omega_{\text{NW}} - \omega_{\text{bulk}}$  over inverse diameter for all optical bulk modes. On the left are the modes of a slab with a thickness of  $20 \text{ \AA}$  which is approximately the diameter of the biggest calculated NW. Top: Phonons belonging to 1-dimensional representations in the bulk. Bottom: Phonons belonging to 2-dimensional representations in the bulk.

be found in other wurtzite crystals as well.<sup>20,21</sup> When treating the vibrations in the zone-folding approximations, it is important to know whether or not there is overbending.<sup>22</sup>

We have plotted a normalized histogram of the  $\Gamma$ -phonons of a representative NW into the bulk phonon density of states (DOS) in Fig. 3. Acoustic modes below  $75 \text{ cm}^{-1}$  are shifted to higher frequencies, whereas the optical modes around  $200 \text{ cm}^{-1}$  are red-shifted, a general trend, *e.g.*, as reported by Sun in Ref.23. There are optical modes in the nanowires with frequencies higher than the LO-mode in the bulk. These modes vibrate mainly on the surface, their frequency exceeding the bulk LO by at most  $15 \text{ cm}^{-1}$ . The reason for the increase lies in the higher coordination of the reconstructed Cd atoms as an inspection of the force constants for the outermost Cd atoms for the slab shows. The sum of the forces on this atom when slightly displaced is higher by 4 % than that of an Cd atom in the center for equal displacement. Force constants of atoms lying in the 2nd layer or closer to the rotational axis do not significantly differ from those in the bulk. This is similar to the subsurface modes predicted for the zirconium surface.<sup>24</sup>

We now turn our attention to optical phonon modes that ex-

ist in bulk material and their counterparts in nanowires. The evolution in phonon frequency with changing nanowire diameter is shown in Fig. 4, where we plot the phonon-frequency difference between the NW and bulk over the inverse diameter. All considered bulk modes that belong to one-dimensional representations show a strong systematic redshift for reduced diameters (upper plot).<sup>23</sup> In contrast, the modes belonging to two-dimensional representations show a smaller size dependence (lower plot). The rigid shift of the  $E_1$ -mode will be explained later. This different size dependence has also been predicted for Si NWs in Ref. 25. They find the LO mode with eigenvectors parallel to the nanowire axis shows a stronger size dependence, than the two TO modes with eigenvectors perpendicular to the axis. This is the same here, all modes belonging to one-dimensional representations have eigenvectors almost parallel to the wire axis and depend strongly on size.

Polar semiconductors are known to have different frequencies for LO and TO modes at the  $\Gamma$ -point. The reason for this is that long-wavelength optical longitudinal atomic vibration induce a polarization field that contributes to the restoring forces due to the long-range Coulomb interaction. It has been shown, that this Coulomb interaction can be treated separately from the short ranged dynamical calculation. In detail the dynamical matrix can be split into an analytical and a non-analytical part, the latter containing the long-range Coulomb forces. Its evaluation is performed as an Ewald summation.<sup>26,27,28</sup> This non-analytical part depends on the unit cell volume and the dielectric high-frequency constant  $\epsilon_{\infty}$ . In bulk CdSe with an experimental dielectric constant<sup>15</sup> of  $\epsilon_{\infty}^{\parallel} = 6.0$  a splitting of  $32 \text{ cm}^{-1}$  is obtained in good agreement with the experimental value of  $39 \text{ cm}^{-1}$ .<sup>2</sup> We apply the same model to nanowires and take the wire cross section times unit cell height as cell volume. To account for the one-dimensionality we only sum over k-vectors along the wire axis. The same dielectric constant  $\epsilon_{\infty}^{\parallel}$  is used.<sup>29</sup> We obtain a splitting of only a few  $\text{cm}^{-1}$  for larger wires; much smaller than in the bulk. We attribute the underestimated splitting to the fact that the displacements within the LO mode in the NW are not well ordered. They are parallel only in the NW-core and even antiparallel near the surface. Consequently the polarization as sum of dipoles becomes weaker compared to bulk. In Fig. 4 the energy difference of the  $A_1$ -modes is calculated without any contribution from the long-ranged Coulomb interactions, neither for bulk nor nanowires. The bulk frequency reference becomes then  $177 \text{ cm}^{-1}$  (calc. with SIESTA). For this mode experimental Raman data is available for nanorods with aspect ratios of  $> 5$  and diameters between 4 and 8 nm.<sup>30,31</sup> A linear fit  $\omega_{\text{NW}} - \omega_{\text{bulk}} = m/d$  leads to  $m = -149 \text{ cm}^{-1} \text{ \AA}$ . The calculated frequencies of the  $A_1$ -modes shown in Fig. 4 are in good agreement with the extrapolated experimental fit.

A rigid shift of the  $E_1$ -mode was predicted by Fuchs and Kliever<sup>32</sup> in a calculation of an ionic crystal slab. They showed that phonons with a polarization perpendicular to the slab surface have frequencies similar to the LO-mode in the bulk. This is attributed to surface charges. A characteristic of this mode is that the Cd and Se sublattices move into opposite directions. To verify this we calculated the phonon frequen-

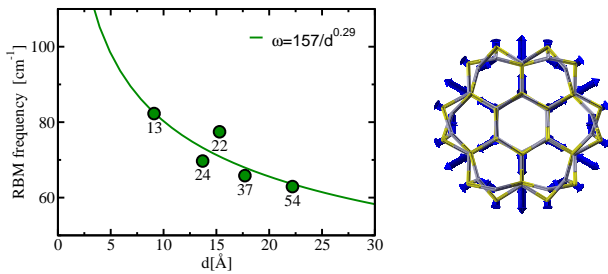


FIG. 5: (Color online) Left: Calculated RBM-frequency (circles). The solid line is a fit  $\omega_{\text{RBM}} = 157/d^{0.29}$ . Right: Displacement pattern of the RBM for the  $(\text{CdSe})_{24}$ -NW.

cies of a thin slab extending into the  $y$  and  $z$ -directions. The non-analyticity is taken along  $z$ . We find that the degeneracy of the  $E_1$ -mode is lifted into two modes: One has a polarization perpendicular to the surface and a frequency of the LO in the bulk; the other one has a polarization vector parallel to the surface and a frequency of the  $E_1$ -mode in bulk. The rigid shift of the  $E_1$  mode in nanowires is thus caused by surface charges in a one-dimensional system and the mode is degenerated again, but now has the frequency of the LO mode in the bulk.

A mode that has no counterpart in the bulk is the radial breathing mode (RBM), where the atoms move almost radially. A representative displacement pattern of the RBM, that of the  $(\text{CdSe})_{24}$ -NW, is shown in Fig. 5. This mode is fully symmetric and should be detectable by Raman experiments. The size dependence of the RBM is important in practical

applications; the size of the NW can be estimated from the measured frequency of the RBM. We tentatively fitted also a  $\omega = A/d^\alpha$  function with the result  $A = 157 \text{ cm}^{-1}\text{\AA}$  and  $\alpha = 0.29$ .

#### IV. SUMMARY

We presented first-principles calculations of CdSe bulk and nanowires. We used an iterative relaxation process that reproduces well the degenerate phonon modes. The effect of a H-passivation on nanowires resulted in smaller unit cells and larger band gaps. We analyzed the vibrational properties of NWs. A reconstruction in the surface leads to higher force constants, resulting in surface modes with frequencies up to  $15 \text{ cm}^{-1}$  higher than in the bulk. The size dependence of phonon modes that correspond to bulk optical  $\Gamma$  modes was analyzed. We find that modes which vibrate mainly along the wire axis showed a stronger size-dependence than modes with eigenvectors perpendicular to the axis. We predict a low-frequency Raman active radial-breathing-like mode that shows a strong diameter dependence and may be used for experimental identification of nanowires.

#### V. ACKNOWLEDGEMENTS

The authors would like to thank M. Machón, H. Scheel and S. Reich for useful discussions; J. M. Pruneda for supplementing the program to calculate the nonanalytic part; H. Lange for providing experimental data prior to publication.

\* Electronic address: marcel@physik.tu-berlin.de

<sup>1</sup> C. Trallero-Giner, A. Debernardi, M. Cardona, E. Menéndez-Proupin, and A. I. Ekimov, *Phys. Rev. B* **57**, 4664 (1998).  
<sup>2</sup> F. Widulle, S. Kramp, N. M. Pyka, A. Göbel, T. Ruf, A. Debernardi, R. Lauck, and M. Cardona, *Physica B* **263**, 448 (1999).  
<sup>3</sup> H. Telg, J. Maultzsch, S. Reich, F. Hennrich, and C. Thomsen, *Phys. Rev. Lett.* **93**, 177401 (2004).  
<sup>4</sup> X. Gonze, J. M. Beuken, R. Caracas, F. Detraux, M. Fuchs, G. M. Rignanese, L. Sindic, M. Verstraete, G. Zerah, F. Jollet, et al., *Computational Materials Science* **25**, 478 (2002).  
<sup>5</sup> X. Gonze, G.-M. Rignanese, M. Verstraete, J.-M. Beuken, Y. Pouillon, R. Caracas, F. Jollet, M. Torrent, G. Zerah, M. Mikami, et al., *Zeit. Kristallogr.* **220**, 558 (2005).  
<sup>6</sup> The ABINIT code is a common project of the Université Catholique de Louvain, Corning Incorporated, and other contributors (<http://www.abinit.org>).  
<sup>7</sup> We used the LDA functional of Perdew and Wang in ABINIT.<sup>34</sup> The valence electrons were expanded in a plane wave basis with an energy cutoff of 30 Hartree. The  $4d$  electrons of Cd were taken as valence. Core electrons were replaced by Troullier-Martins pseudopotentials.<sup>12</sup> A shifted  $10 \times 10 \times 4$  sampling grid was used for the integration over the Brillouin zone. The dynamical matrix was calculated on a  $10 \times 10 \times 4$   $q$ -grid. Force constants were obtained via a Fourier transformation and interpolated to obtain phonons at arbitrary points in the Brillouin zone. The splitting of the LO and TO phonons was calculated with the standard model.<sup>26,27</sup> ABINIT yields a dielectric high-frequency constant

of  $\epsilon_\infty^{\parallel} = 7.2$ .

<sup>8</sup> P. Ordejón, E. Artacho, and J. M. Soler, *Phys. Rev. B* **53**, R10 441 (1996).  
<sup>9</sup> J. M. Soler, E. Artacho, J. D. Gale, A. García, J. Junquera, P. Ordejón, and D. Sánchez-Portal, *J. Phys. Condens. Mat.* **14**, 2745 (2002).  
<sup>10</sup> D. M. Aruguete, M. A. Marcus, L. S. Li, A. Williamson, S. Fakra, F. Gygi, G. A. Galli, and A. P. Alivisatos, *J. Phys. Chem. C* **111**, 75 (2007).  
<sup>11</sup> J. P. Perdew and A. Zunger, *Phys. Rev. B* **23**, 5048 (1981).  
<sup>12</sup> N. Troullier and J. L. Martins, *Phys. Rev. B* **43**, 1993 (1991).  
<sup>13</sup> H. J. Monkhorst and J. D. Pack, *Phys. Rev. B* **13**, 5188 (1976).  
<sup>14</sup> M. T. Yin and M. L. Cohen, *Phys. Rev. B* **26**, 3259 (1982).  
<sup>15</sup> H. W. Verleur and A. S. Barker Jr., *Phys. Rev.* **155**, 750 (1967).  
<sup>16</sup> D. Fernández-Torre, R. Escribano, T. Archer, J. M. Pruneda, and E. Artacho, *J. Phys. Chem. A* **108**, 10535 (2004).  
<sup>17</sup> B. Bonello and B. Fernandez, *J. Phys. Chem. Solids* **54**, 209 (1993).  
<sup>18</sup> M. Vujčić, *J. Phys. A: Math. Gen.* **10**, 1271 (1977).  
<sup>19</sup> H. Yu, J. B. Li, R. A. Loomis, P. C. Gibbons, L. W. Wang, and W. E. Buhro, *J. Amer. Chem. Soc.* **125**, 16168 (2003).  
<sup>20</sup> T. Ruf, J. Serrano, M. Cardona, P. Pavone, M. Pabst, M. Krisch, M. D'Astuto, T. Suski, I. Grzegory, and M. Leszczynski, *Phys. Rev. Lett.* **86**, 906 (2001).  
<sup>21</sup> J. Serrano, A. H. Romero, F. J. Manjon, R. Lauck, M. Cardona, and A. Rubio, *Phys. Rev. B* **69**, 094306 (2004).  
<sup>22</sup> H. Richter, Z. P. Wang, and L. Ley, *Solid State Commun.* **39**, 625

- (1981).
- <sup>23</sup> C. Q. Sun, Prog. Solid State Chem. **35**, 1 (2007).
- <sup>24</sup> M. Yamamoto, C. T. Chan, K. M. Ho, M. Kurahashi, and S. Naito, Phys. Rev. B **53**, 13772 (1996).
- <sup>25</sup> L. Yang, Ph.D. thesis, Georgia Institute of Technology (2006).
- <sup>26</sup> W. Cochran and R. A. Cowley, J. Phys. Chem. Solids **23**, 447 (1962).
- <sup>27</sup> P. Giannozzi, S. de Gironcoli, P. Pavone, and S. Baroni, Phys. Rev. B **43**, 7231 (1991).
- <sup>28</sup> M. Born and K. Huang, *Dynamical Theory of Crystal Lattices* (Oxford University Press, 1954).
- <sup>29</sup> G. D. Mahan, Phys. Rev. B **74**, 033407 (2006).
- <sup>30</sup> H. Lange, M. Machón, M. Artemyev, U. Woggon, and C. Thomsen, phys. stat. sol. (RRL) **1**, 274 (2007).
- <sup>31</sup> H. Lange (priv. comm. (2008)).
- <sup>32</sup> R. Fuchs and K. L. Kliewer, Phys. Rev. **140**, A2076 (1965).
- <sup>33</sup> T. Thonhauser and G. D. Mahan, Phys. Rev. B **71**, 081307(R) (2005).
- <sup>34</sup> J. P. Perdew and Y. Wang, Phys. Rev. B **45**, 13244 (1992).